A normalized description of the direct effect of key aerosol types on solar radiation as estimated from Aerosol Robotic Network aerosols and Moderate Resolution Imaging Spectroradiometer albedos

Mi Zhou,[1] H. Yu,[2] R. E. Dickinson,[1] O. Dubovik,[3] and B. N. Holben[3]

Received 23 February 2005; revised 10 May 2005; accepted 30 June 2005; published 5 October 2005.

[1] The interactions between aerosols and solar radiation are determined by a combination of aerosol properties (i.e., types), surface properties (i.e., albedo) and clouds. These determining factors vary for different regions. We examine how these differences contribute to the impact of aerosols on the top-of-atmosphere (TOA) and surface radiation. In this study, the AERONET (Aerosol Robotic Network) aerosol climatology is used, in conjunction with surface albedo and cloud products from Moderate Resolution Imaging Spectroradiometer (MODIS), to calculate the aerosol direct radiative effect (ADRE) and its normalized form (NADRE). The NADRE is defined as the ADRE normalized by optical depth at 550 nm and is mainly determined by internal aerosol optical properties and geographical parameters. These terms are evaluated for cloud-free and cloudy conditions and for all-mode and fine-mode aerosols. Single-scattering albedo is an important variable determining ADRE of biomass burning. Because of stronger absorption by the smoke over South Africa the average NADRE over South America is ~35% larger at the TOA but ~38% smaller at the surface than that over South Africa. The surface albedo is another important factor in determining ADRE, especially for mineral dust. As the surface albedo varies from ~0.1 to ~0.35, it is observed that the dust NADRE ranges from −44 to −17 $Wm^{-2}\,\tau^{-1}$ at the TOA and from −80 to −48 $Wm^{-2}\,\tau^{-1}$ at the surface over the Saharan deserts, Arabian Peninsula, and their surrounding oceans. We also find that the NADRE of fine-mode aerosol is larger at the TOA but smaller at the surface in comparison to that of all-mode aerosol because of its larger single-scattering albedo and smaller asymmetry factor. Cloudy-sky ADRE is usually not negligible for the observed cloud optical thickness, but the TOA ADRE with clouds is sensitive to the relative location of aerosols and cloud layer.

Citation: Zhou, M., H. Yu, R. E. Dickinson, O. Dubovik, and B. N. Holben (2005), A normalized description of the direct effect of key aerosol types on solar radiation as estimated from Aerosol Robotic Network aerosols and Moderate Resolution Imaging Spectroradiometer albedos, *J. Geophys. Res.*, *110*, D19202, doi:10.1029/2005JD005909.

1. Introduction

[2] Aerosols modify the Earth-atmosphere energy budget through scattering and absorption (the so-called direct effect) [*Bohren and Huffman*, 1983; *Coakley et al.*, 1983; *Charlson et al.*, 1992], by changing atmospheric thermodynamics and cloud formation (the so-called semidirect effect) [*Hansen et al.*, 1997; *Ackerman et al.*, 2000; *Koren et al.*, 2004], and by changing cloud microphysics (the so-called indirect effects) [*Twomey*, 1977; *Albrecht*, 1989; *Rosenfeld and Lensky*, 1998]. Radiative forcing by aerosols is a critical component of the global and regional climate because of its influence on land surface and atmospheric boundary layer processes [*Yu et al.*, 2002], global surface temperatures [*Coakley et al.*, 1983; *Charlson et al.*, 1992], climate and the hydrological cycle [*Ramanathan et al.*, 2001], and ecosystems [*Chameides et al.*, 1999]. The cooling by anthropogenic aerosols may be comparable in magnitude to greenhouse gas warming on a global scale but can be much larger on a regional scale [*Intergovernmental Panel on Climate Change* (*IPCC*), 2001]. However, uncertainties remain substantial for the direct effect and even much larger for the indirect effect [*IPCC*, 2001; *Anderson et al.*, 2003a].

[3] Until recently, estimates of the global impact of aerosols on climate were primarily based on model results that were evaluated using local aerosol measurements (see summary given by *Haywood and Boucher* [2000]). Recently, significant progress has been achieved in measurement-based aerosol characterization from satellite remote sensing, surface networks, aircraft and in situ

[1] School of Earth and Atmospheric Sciences, Georgia Institute of Technology, Atlanta, Georgia, USA.
[2] Goddard Earth Science and Technology Center, NASA Goddard Space Flight Center and University of Maryland Baltimore County, Greenbelt, Maryland, USA.
[3] NASA Goddard Space Flight Center, Greenbelt, Maryland, USA.

0148-0227/05/2005JD005909$09.00

measurements. A ground-based remote sensing network equipped with well-calibrated sunphotometers over more than 100 sites throughout the world, the Aerosol Robotic Network (AERONET), measures and derives quality-assured aerosol optical properties for a wide diversity of aerosol regimes, for up to the last 10 years, including spectral variations of aerosol optical depth, single-scattering albedo, the phase function/asymmetry factor for both fine-mode and coarse-mode aerosols [*Holben et al.*, 1998, 2001; *Dubovik et al.*, 2002]. These high-quality data have been widely used for aerosol process studies and evaluation and validation of model simulation and satellite remote sensing of aerosols [*Chin et al.*, 2002; *Yu et al.*, 2003; *Remer et al.*, 2005]. The separation of fine-mode from coarse-mode aerosol properties as done by AERONET provides a possible way to estimate the anthropogenic aerosol direct forcing because anthropogenic aerosols are overwhelmingly concentrated in the fine-mode [*Kaufman et al.*, 2002]. However, most fine-mode particles are not necessarily anthropogenic. How to derive anthropogenic aerosol direct forcing by making use of fine-mode aerosol information needs further study [*Anderson et al.*, 2005].

[4] How aerosols modify solar radiation is strongly influenced by surface albedo [*Coakley et al.*, 1983; *Haywood and Shine*, 1995, 1997]; this interaction leads to complicating multiple reflections. An inadequate specification of the highly heterogeneous land surface albedos [*Dickinson*, 1983] may thus introduce additional uncertainties in aerosol direct forcing [*Collins et al.*, 2002]. Surface albedos for climate radiation studies have usually been calculated from land models based on empirical parameterizations of vegetation and soils [*Dickinson et al.*, 1993; *Sellers et al.*, 1996]. To avoid the significant error that such an approach may entail, we use albedos from the Moderate Resolution Imaging Spectroradiometer (MODIS), whose multispectral capability allows for better atmospheric correction [*Vermote et al.*, 2002] and improves the quality of the retrieved land albedo data for direct and diffuse radiation [*Schaaf et al.*, 2002].

[5] It is feasible and important to generate a measurement-based climatology of the aerosol direct effect that will serve for evaluating both satellite-based and model-based forcing. For a specific type of aerosol, its particle size distribution, chemical composition and shape determine the internal aerosol optical properties, including the wavelength dependence of optical depth, single-scattering albedo, and asymmetry factor; however there can be large variability in aerosol radiative effect even under the same geographical conditions, because of large variations of aerosol optical depth with time [*Anderson et al.*, 2003b]. A normalization of aerosol direct radiative effect with optical depth can remove much of the influence of optical depth variation. In this study, the AERONET aerosol climatology, in combination with land surface albedo and cloud properties derived from MODIS, is used to calculate the aerosol direct radiative effect normalized by optical depth at 550 nm at the top-of-atmosphere (TOA) and surface, under cloud-free and cloudy conditions. Section 2 describes the AERONET aerosol climatology and MODIS data, model calculations and methods used for analysis. The derived aerosol direct effect on solar radiation is discussed in section 3. Specifically, the discussion focuses on the distinctions of aerosol direct effect between different aerosol regimes, between fine-mode and coarse-mode, and between clear sky and cloudy sky. Major results are concluded in section 4.

2. Description of Data and Model Calculations

2.1. Data

[6] The AERONET program is an inclusive federation of ground-based aerosol remote sensing network around the world with more than 100 sites for up to 10 years [*Holben et al.*, 1998, 2001]. Spectral measurements from sunphotometers and sky radiance radiometers are calibrated and screened for cloud-free conditions [*Smirnov et al.*, 2000]. Flexible algorithms have been developed to derive the columnar integrated and spectral-resolved aerosol optical properties in distinct aerosol regimes [*Holben et al.*, 1998, 2001; *Dubovik and King*, 2000; *Dubovik et al.*, 2000, 2002]. The data used in this study are cloud-screened and quality-assured (Level 2.0) monthly aerosol climatology, including optical depth, single-scattering albedo, and asymmetry factor at 440, 670, 870, 1020 nm for both fine-mode aerosol and all-mode (including fine-mode and coarse-mode) aerosol. The wavelength dependence of optical depth is described by an Ångstrom exponent, which is calculated as the linear regression slope $-\ln\tau/\ln\lambda$, where τ is optical depth and λ is wavelength.

[7] It should be noted that the inversion-based retrievals of single-scattering albedo and asymmetry factor have yet to be systematically validated by in situ measurements, so we simply take their standard deviations as uncertainties [*Dubovik et al.*, 2002] to study the associated uncertainties in aerosol forcing estimation. For single-scattering albedo, uncertainties are $\pm 0.01 \sim \pm 0.03$ for all major types of aerosols; for asymmetry factor, uncertainties are $\pm 0.03 \sim \pm 0.08$ for pollution and biomass burning aerosol and ± 0.04 for dust. These uncertainties generally transform to aerosol forcing uncertainties of $\sim 15-20\%$ at the TOA and $\sim 10\%$ at the surface. One exception is associated with uncertainties of dust single-scattering albedo over high reflective surface (albedo $\sim 0.3-0.35$). The interaction of dust absorption with high surface reflection magnifies the aerosol forcing uncertainties to $\sim 60\%$ at the TOA and $\sim 20\%$ at the surface. However, the magnitude of TOA forcing in this case is relatively small and the absolute uncertainty may not be large.

[8] AERONET aerosol optical properties at the four wavelengths are linearly interpolated or extrapolated to the radiation model spectral divisions. The single-scattering albedo, asymmetry factor and Ångstrom exponent at wavelengths longer than 1020 nm are taken as the observed values at 1020 nm. The spectral single-scattering albedo of polluted aerosol with a certain amount of soot drops rapidly at around 2000 nm [*Hess et al.*, 1998]. We conducted a sensitivity study that decreases single-scattering albedo to 0.2 at 1900 nm and beyond, and found that the introduced uncertainty in solar radiative effect is within 8% at the TOA and 3% at the surface. A factor 2 of change in the Ångstrom exponent at wavelengths beyond 1020 nm would lead to an uncertainty less than 5%. The radiation model [*Fu and Liou*, 1993] simplifies the phase function by use of an asymmetry factor. Such simplification might introduce large errors (up

to 20%) in aerosol forcing calculation, depending on solar zenith angle, aerosol size distribution and refractive index [*Boucher*, 1998]. However, it is problematic to estimate the overall uncertainty because of a lack of knowledge about possible correlations between individual uncertainties. We might take 20% as a rough estimate as this term is expected to dominate over the 5% and 8% terms. Our sensitivity tests also show that using aerosol properties in the visible only would overestimate the aerosol solar radiative effect by about 20% at the TOA and 10% at the surface.

[9] A calculation of the aerosol direct radiative effect requires information on surface albedo and clouds such as those obtained from MODIS retrievals. Over land, visible and near-infrared broadband (namely, 0.3∼0.7 μm and 0.7 ∼4 μm) surface albedos are taken from MODIS monthly retrievals of white-sky albedo for 2001 [*Schaaf et al.*, 2002]. The solar zenith angle and details of spectral dependence of land albedo are thus not considered. *Yu et al.* [2004] account for the angular dependence of surface albedo by simply weighted black-sky and white-sky albedo with the direct beam fraction and diffuse light fraction, respectively. Because of change of the direct beam fraction by aerosols, the calculated surface reflection with the presence of aerosol is different from that without aerosol, contributing to the aerosol direct effect at the TOA. They concluded that the neglect of angular dependence of surface albedo will introduce an uncertainty that is small (i.e., less than 5%) for monthly and global average but can be more significant for the diurnal cycle of aerosol TOA forcing. In comparison to ground-based albedometer measurements over semidesert region, it is shown that MODIS albedo has accuracy of ±0.05 and mostly close to ±0.02 [*Lucht et al.*, 2000]. Given ±0.05 uncertainty in surface albedo, an introduced uncertainty in dust forcing is ∼40% at the TOA and ∼10% at the surface over semidesert region with albedo ∼0.3–0.35. Please note again the TOA forcing in this case is relatively small in magnitude and so the absolute uncertainty may not be large. The uncertainties in aerosol forcing associated with MODIS albedo are expected to be much smaller for most other regions because semidesert regions have relatively large albedo values. For example, ±0.05 change in albedo of ∼0.2 only introduces the dust forcing change of ∼15% at the TOA and ∼5% at the surface. The near-infrared broadband albedo is an adequate specification for soil. However, it underestimates average grass albedo over 0.7–1.3 μm by about 10% because of a sharp drop in albedo at around 1.3 μm (http://www-surf.larc.nasa.gov/surf/pages/explan.html). The associated overestimation in aerosol direct effect is <7% at the TOA and <2% at the surface for grassland but can be larger for a snow covered surface. Therefore a more detailed spectral surface albedo may be needed to better characterize the aerosol effect over vegetation and snow. Over ocean, the increase of surface albedo with solar zenith angle is accounted for by a look-up table that is generated by a coupled atmosphere-ocean radiative transfer model [*Jin et al.*, 2002, 2004]. The dependence of albedo on wind speed and chlorophyll concentration is not considered. This assumption introduces a relatively small uncertainty (less than 10%) in diurnal average of aerosol solar effect because a change of chlorophyll concentration from 0 to 10 mg m^{-3} only changes the broadband ocean albedo by less than 0.005 and the increasing ocean albedo with wind speed depends on solar zenith angle [*Yu et al.*, 2004].

[10] The daytime file of MODIS/Terra level 3 monthly $1^\circ \times 1^\circ$ cloud products (MOD08M3) is used in this study, including water cloud optical depth, ice cloud optical depth, and cloud fraction for year 2001 [*King et al.*, 2003; *Platnick et al.*, 2003]. It represents the atmospheric state at local time 10:30am. There are also MODIS/Aqua cloud data (MYD08M3) representing the state at 1:30pm. Difference between these two may suggest part of diurnal variations. In our sensitivity tests, we do not account for such diurnal variation. An effective radius is assumed to be 10 μm for water cloud and 50 μm for ice cloud [*Liao and Seinfeld*, 1998; *Fu and Liou*, 1993].

2.2. Model Calculations and Methods of Analysis

[11] The AERONET aerosol data and MODIS surface albedo discussed above are used as inputs to a broadband delta-four-stream radiation model [*Fu and Liou*, 1993] to calculate the net solar fluxes at both the TOA and surface under cloud-free conditions. How aerosols affect thermal infrared radiation is important for mineral dust, but is not addressed here. The climatology from *McClatchey et al.* [1972] is taken for average atmospheric conditions in our calculation. This choice of temperature, water vapor and ozone profiles has a small influence on the calculation of aerosol solar radiative effect [*Boucher et al.*, 1998; *Yu et al.*, 2004]. The model is run over a 24-hour diurnal cycle with solar insolation of the 15th day of each month. A time step of 30 min is applied to adequately capture the solar zenith angle dependence of the aerosol radiative effects and hence to provide a monthly average [*Yu et al.*, 2004]. Model runs with and without aerosols are compared to estimate the aerosol direct radiative effect (ADRE).

[12] To facilitate discussion, we define the NADRE as the normalized ADRE by the optical depth at 550 nm (the average value of observed optical depth at 440 and 670 nm) at both the TOA and surface. By doing so, we remove much of the influence of aerosol loading and so see more clearly how the ADRE can be impacted by the internal aerosol optical properties, determined by the particle size distributions, chemical compositions and shape. Different types of aerosols have different size distributions and chemical compositions. The major types distinguished here include biomass burning, dust, industrial pollution as listed in Table 1. Table 1 also lists the selected AERONET sites with a complete and reasonable annual cycle that we could use to represent regions influenced by those distinct aerosol types. Figure 1 shows the corresponding optical properties, including mean values, which is the average over time and selected sites for each category, and standard deviations. The relatively large spread in optical depth illustrates the large spatial and temporal variation. Thus it is necessary to look at the NADRE to see dependences on other aerosol optical properties.

[13] The calculated NADRE must be used with caution when extrapolating or comparing to other studies, because the ADRE is a nonlinear function of aerosol optical depth. The NADRE decreases with optical depth at high solar zenith angle and increases at low solar zenith angle, therefore its variability is partially canceled out when averaging over solar zenith angle. For surface albedo of

Table 1. Selected AERONET Stations for Stratifying the Data Into Different Aerosol Types and Geographical Regions

Aerosol Types	Regions	AERONET Stations
Biomass burning	South America	Alta_Floresta
Biomass burning	South Africa	Mongu and Skukuza
Mineral dust	albedo < 0.1	Capo_verde and Baharain
Mineral dust	albedo ~ 0.2	Ilorin and Nes_Ziona
Mineral dust	albedo 0.3 ~ 0.35	Banizoumbou, SEDE_BOKER, Solar_Village
Pollution	North America	COVE, GSFC, MD_Science_Center, Oyster, SERC, Stennis, Wallops
Pollution	west Europe	Ispra, Lille, Moldova and Venise
Pollution	east Asia	Anmyon, NCU_Taiwan, Shirahama

0.15 and single-scattering albedo of 0.95, because of the nonlinearity, an increase of 0.25 in optical depth would decrease 0°–90° solar-zenith-angle-averaged clear-sky NADRE by 7% at the TOA and 3% at the surface. For single-scattering albedo of 0.8, the 0°–90° solar-zenith-angle-averaged clear-sky NADRE is changed by a very small value at the TOA and 5% at the surface (Figure 2). The distribution of solar zenith angle at a certain location depends on the latitude and season, hence the change in clear-sky NADRE with aerosol optical depth can be larger at high latitudes or in winter season. The relative error in average ADRE derived from average NADRE and average optical depth is generally less than 7% for categories listed in Table 1 except for South America biomass burning, which is limited by lack of data (only one selected site) and so has a much larger variation in optical depth than others. The relationship of ADRE with optical depth becomes more linear when clouds are present, probably resulting from in-cloud multiscattering, and improved linearity with larger cloud optical depth.

[14] Under clear skies, the vertical distribution of absorbing aerosols are important for calculating backscattered UV, however, it becomes unimportant over the whole solar spectrum even for absorbing aerosols. Thus we assume a well-mixed profile within the lowest 2 km layer. Under cloudy skies, on the other hand, the radiative effect of aerosol depends highly on the relative distributions of aerosols and cloud layer in the vertical [*Liao and Seinfeld*, 1998; *Keil and Haywood*, 2003]. Because MODIS doesn't provide such information, sensitivity tests have been carried out by using two idealized aerosol-cloud profiles to examine how ADRE is sensitive to aerosol-cloud distributions. In either case, ice clouds are assumed to stay above the aerosol layer. In one test, denoted as the below-cloud case, we assume that the water cloud is completely above the aerosol layer. In the other test denoted as the within-cloud case, 50% of aerosol extinction is assumed below the water cloud and the remaining is above the water cloud. In two cases, the columnar optical depth of aerosol is the same. The MODIS cloud fraction (f_{cld}) is used to weigh aerosol

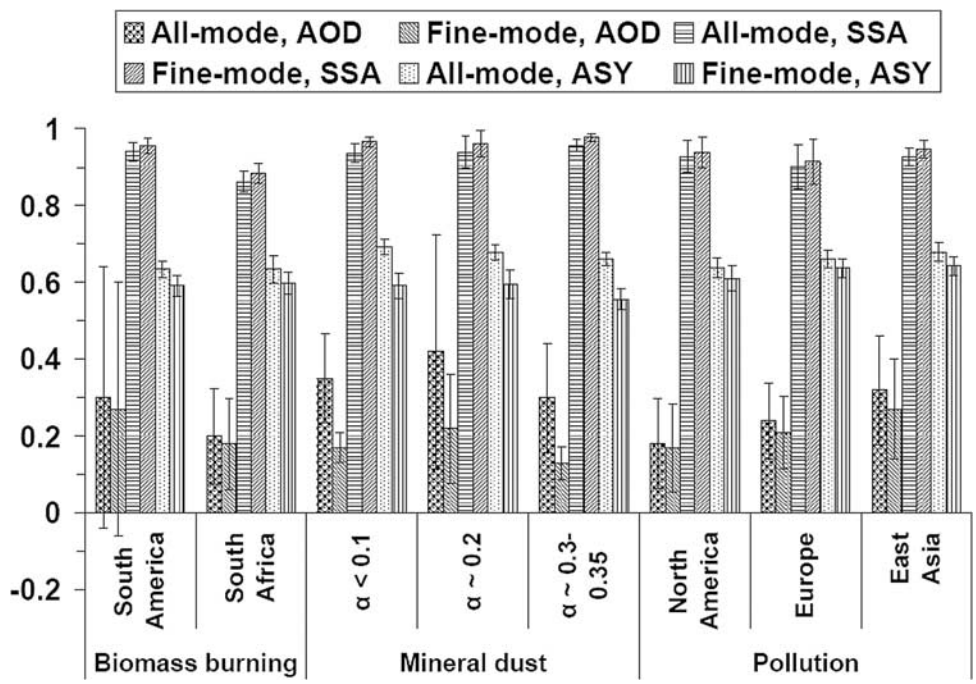

Figure 1. Mean values and standard deviations of aerosol optical depth (AOD), single-scattering albedo (SSA) and asymmetry factor (ASY) at 550 nm for typical aerosol types and over different geographical regions, where α is surface albedo. Standard deviation is shown as the error bar. Values less than zero can be regarded as equivalent to about zero.

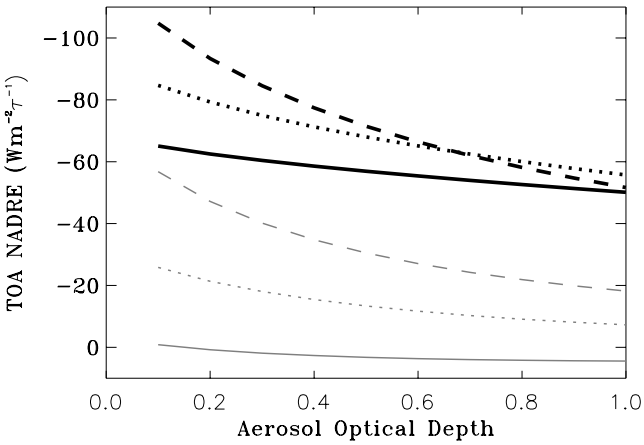

Figure 2. How normalized aerosol direct radiative effect (NADRE, unit: Wm^{-2} τ^{-1}) averaged over solar-zenith angles changes with aerosol optical depth at the TOA for surface albedo of 0.15 and single scattering albedo of 0.95 (solid) and 0.8 (shaded), respectively, and over different solar zenith angle ranges of 0°–90° (solid line), 30°–90° (dotted line) and 60°–90° (dashed line).

cloudy-sky NADRE (NADRE_cld) and clear-sky NADRE (NADRE_clr) to generate all-sky NADRE (NADRE_all), as follows:

$$\text{NADRE\_all} = f_{cld}\text{* NADRE\_cld} + (1 - f_{cld})\text{*NADRE\_clr} \quad (1a)$$

or

$$\text{NADRE\_all/NADRE\_clr} = f_{cld}\text{* NADRE\_cld/NADRE\_clr} + (1 - f_{cld}) \quad (1b)$$

Equation (1b) suggests that all-sky to clear-sky NADRE can be larger, equal to, or smaller than the clear-sky fraction ($1 - f_{cld}$), depending on aerosol and cloud properties that determine the sign and value of cloudy-sky NADRE.

[15] The radiative calculations have been conducted for each of the 203 AERONET sites with annual aerosol climatology. The so-derived climatology of monthly aerosol direct radiative effects can serve as a baseline product to evaluate the assessment of aerosol radiative effect based on satellite retrievals, model simulations or an integration of satellite and modeling [*Boucher and Tanre*, 2000; *Chou et al.*, 2002; *Yu et al.*, 2004; *Zhang et al.*, 2005]. The following discussion will focus on comparisons of aerosol radiative effects between different aerosol types (e.g., biomass burning, mineral dust, and pollution), geographical locations (South America, South Africa, North America, west Europe, and east Asia), and surface properties (e.g., large variations of surface albedo in Saharan deserts and Arabian peninsula), as listed in Table 1.

3. Results and Discussion

3.1. Cloud-Free NADRE by All-Mode Aerosol

[16] Clear-sky aerosol forcing is determined by geographically varying aerosol optical properties and geophysical parameters, such as surface albedo. Such variations are illustrated in the following through discussion of major aerosol types using the categories listed in Table 1. Mean values with standard deviations for the NADRE at the TOA and surface are shown in Figure 3, where standard deviations represent monthly and spatial variations in NADRE. Also shown in Figure 3 is the NADRE for fine-mode aerosols, which will be discussed in section 3.2.

[17] Biomass burning occurs mainly in the tropics during the dry season [*Delmas et al.*, 1991]. Single-scattering albedo of biomass burning smoke varies significantly with different black carbon content because of different aging processes, source and meteorological characteristics [*Dubovik et al.*, 2002; *Eck et al.*, 2003]. A much stronger absorption is observed for African savanna fires than for Amazonian forest fires [*Dubovik et al.*, 2002; *Eck et al.*, 2003]. The average single-scattering albedo at 550 nm is 0.940 ± 0.025 in South America, compared to 0.862 ± 0.027 in South Africa, according to the data presented in this study. Such differences in smoke absorption result in different NADREs because aerosol absorption reduces the upscattering component at the TOA (i.e., a smaller TOA cooling) and absorbs solar energy in the atmosphere that otherwise can reach the surface (i.e., a larger surface cooling). On average, the NADRE in South America is larger at the TOA by 35% (more negative) and smaller at the surface by 38% (less negative) than those in South Africa. As shown in Figure 4, the ratio of TOA to surface NADRE generally decreases with decrease of aerosol single-scattering albedo, and so readily separates biomass burning aerosol in South Africa (triangles) from South America (circles); thus it provides an alternative to single-scattering albedo for such distinction. In South America, the TOA to surface NADRE ratio decreases from about 0.81 to 0.39 with single-scattering albedo ranging from 0.99 to 0.91. In South Africa, the single-scattering albedo ranges from 0.90 to 0.81 and the corresponding TOA to surface NADRE ratio ranges from 0.36 to 0.14.

[18] Mineral dust dominates aerosol radiative effect over North Africa and the Arabian Peninsula where the surface reflectivity is high and has considerable spatial variability, ranging from about 0.2 to 0.4 for broadband albedo [*Tsvetsinskaya et al.*, 2002]. Dust outflows also substantially influence radiation absorbed by nearby oceans where the surface albedo is less than 0.1. The large variability of surface albedo significantly influences the ADRE of mineral dust, as shown in Figures 3 and 5. The net surface solar flux is a product of downward solar flux reaching the surface and $(1 - \alpha)$, where α is the surface albedo. As such, with the same aerosol properties and hence the same changes of downward solar flux, the ADRE at the surface decreases with increasing surface albedo. Moreover, aerosols absorb as well as scatter back the surface-reflected solar radiation through multiple reflections between the surface and aerosol layer. As the surface albedo increases, both TOA and surface NADRE decrease significantly. This trend can easily be seen from the average values in Figure 3. Note that climatological differences in aerosol properties over different surfaces also introduce differences in dust solar radiative effect as shown in Figure 3. Comparisons of single-scattering albedo and asymmetry factor suggest that aerosol over dark oceans is slightly more absorbing and larger in size than that over the brightest surface. Since these

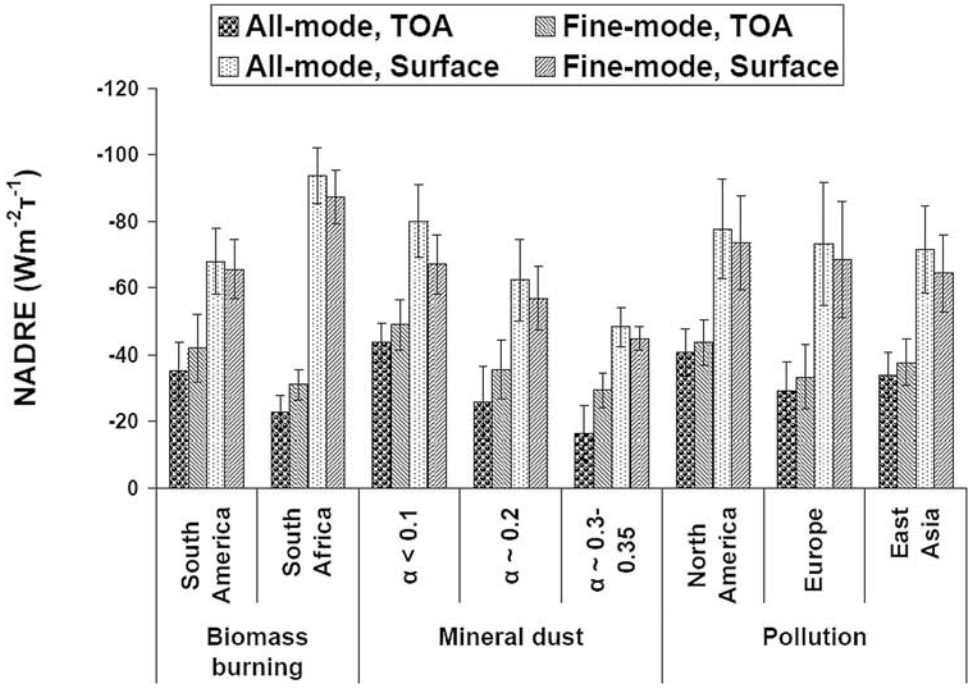

Figure 3. Mean values and standard deviations of clear-sky normalized aerosol direct radiative effect (NADRE) at the TOA and surface (unit: Wm^{-2} τ^{-1}) for typical aerosol types and over different geographical regions, where standard deviations represent monthly and spatial variations in NADRE and α is surface albedo.

differences are relatively small and have compensating effects on aerosol solar radiative effect at the surface, they should not be major factors contributing to the differences illustrated in Figure 3. Therefore we conclude that the much reduced aerosol TOA and surface radiative effects for high reflective surfaces (i.e., with the albedo of 0.3 to 0.35), about 38% and 60% respectively of that over ocean (i.e., albedo of less than 0.1), are mainly determined by the differences in surface albedo. This conclusion is further corroborated by the fact that the change of TOA to surface NADRE ratio with single-scattering albedo is well separated by the surface albedo, as shown in Figure 5. The ratio of TOA to surface NADRE decreases with the decreasing single-scattering albedo more rapidly over a high surface albedo than over a low surface albedo.

[19] In North America, Europe, and east Asia, the urban-industrial pollution perturbs the solar radiation appreciably, as shown in Figure 3. The NADRE by industrial aerosol in Europe demonstrates a wider range and larger variation with larger standard deviation than that in North America and

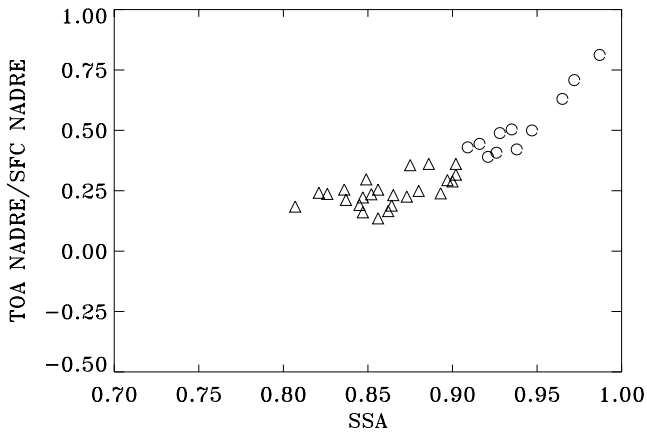

Figure 4. Ratio of TOA NADRE to surface (SFC) NADRE decreasing with decreasing aerosol single-scattering albedo (SSA) for biomass burning smoke over South America (circles) and over South Africa (triangles), respectively.

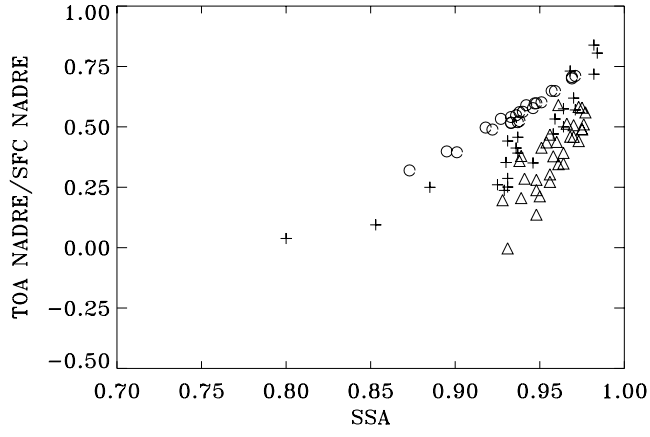

Figure 5. Ratio of TOA NADRE to surface (SFC) NADRE decreasing with decreasing aerosol single-scattering albedo (SSA) for mineral dust. The data are stratified with the solar spectrum surface albedo, with circles, pluses, and triangles denoting the surface albedo α of <0.1, ~0.2, and 0.3~0.35, respectively.

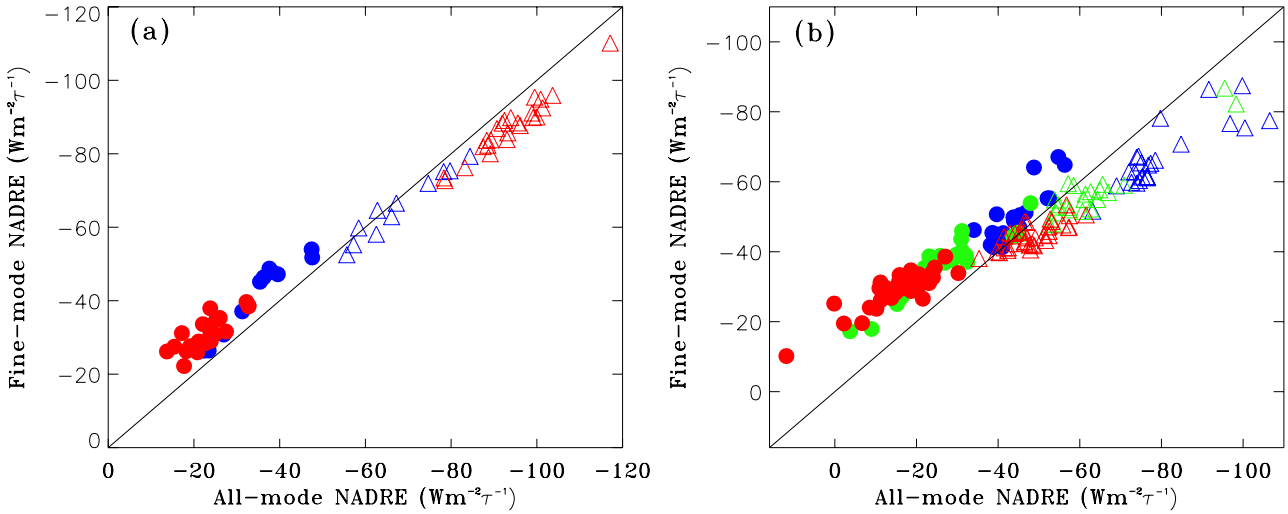

Figure 6. Comparisons of fine-mode and all-mode aerosol NADRE (unit: $Wm^{-2}\,\tau^{-1}$) at the TOA (dots) and surface (triangles) for (a) biomass burning aerosol, with blue and red representing South America and South Africa, respectively, and (b) mineral dust, with blue, green and red representing the surface albedo $\alpha < 0.1$, ~0.2, ~0.3–0.35, respectively.

east Asia. On average, the TOA and surface NADRE is relatively large in North America.

3.2. Cloud-Free NADRE by Fine-Mode Aerosol

[20] In comparison to coarse-mode and all-mode aerosol, the fine-mode aerosol has a larger surface per unit volume and is closer in size to wavelength of maximum solar energy. Thus it should have a smaller absorption (i.e., larger single-scattering albedo) and a smaller forward scattered fraction (i.e., smaller asymmetry factor) for the same chemical composition. The fine-mode aerosol also has a larger wavelength dependence (i.e., larger Ångstrom exponent) than the all-mode aerosol does. Our calculations show that the Ångstrom exponent has a relatively small effect (e.g., within 7%) on aerosol direct effect, because of compensating effects at shorter and longer solar wavelength. As such, differences between fine-mode and all-mode NADRE are largely determined by differences in the single-scattering albedo and asymmetry factor as shown in Figure 1. For fine-mode aerosols, the smaller absorption increases the NADRE at the TOA but decreases it at the surface; the larger portion of backscattering or the smaller asymmetry factor increases the NADRE at both the TOA and surface. As such, distinctions between the fine-mode and all-mode aerosol NADRE should vary at the TOA and at the surface and should depend on aerosol types, as shown in Figure 6. The average values are shown in Figure 3.

[21] Figure 6a shows that the biomass burning NADRE at the TOA for fine-mode aerosols is larger than that by all-mode aerosols, but they are close at the surface because more upscattering and less absorbing by fine particles are added at the TOA but offset at the surface. The ratio of average NADRE of fine-mode to all-mode aerosol is 1.20/1.36 at the TOA and 0.97/0.93 at the surface for South America/South Africa aerosols. The difference in asymmetry factor between fine-mode and all-mode aerosols is larger for mineral dusts than those of biomass burning and industrial aerosols. The fine-mode dust NADRE is larger at the TOA and smaller at the surface (Figure 6b). According to Figure 3, the ratio of fine-mode to all-mode aerosol average NADRE increases at the TOA (1.2, 1.4, 1.8) and at the surface (0.83, 0.91, 0.93) as surface albedo increases (0.1, 0.2, 0.3–0.35) because of the radiative interactions of surface reflection with aerosols. Similar to biomass burning aerosol and mineral dust, fine-mode NADRE for pollution aerosol is also larger at TOA but smaller at surface than all-mode NADRE. The NADRE difference between fine-mode and all-mode aerosol is relatively small, partially because of the high fine-mode fraction in industrial region.

[22] Anthropogenic aerosols are generally fine particles and it has been proposed to use the fine-mode fraction derived from satellite observations and ground-based measurements to estimate the anthropogenic aerosol radiative forcing [*Kaufman et al.*, 2002]. As discussed earlier, the NADRE differs substantially between fine-mode and all-mode aerosols. Note also that the AERONET-derived fine-mode aerosol properties may not well represent those of anthropogenic aerosols, because only one retrieved refractive index is assumed for particles of all sizes [*Dubovik et al.*, 2000]. As such all-mode aerosol is more absorbing than fine-mode aerosol from AERONET retrievals. Thus additional information besides the fine-mode fraction is needed to derive anthropogenic aerosol forcing [*Anderson et al.*, 2005].

3.3. Cloudy Sky and All Sky NADRE by All-Mode Aerosol

[23] Clouds can modify aerosol direct radiative effect, depending on cloud optical properties such as cloud fraction, cloud optical depth and the relative position of the cloud layer with aerosols. For each category in Table 1, Figure 7 shows the ratios of average cloudy-sky to clear-sky NADRE for below-cloud and within-cloud cases with the average total cloud optical depth (TCOD) and water cloud optical depth (WCOD). In the below-cloud case, the cloudy-sky NADRE is smaller than the corresponding value for clear-sky, depending mainly on the total optical depth of cloud. With an increase of cloud optical depth, the amount

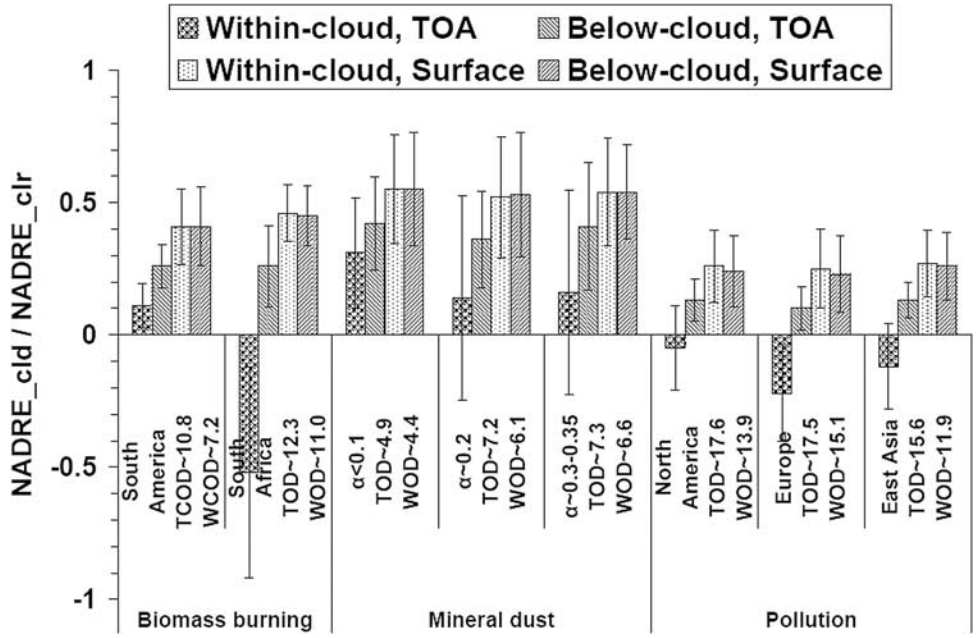

Figure 7. Ratio of average cloudy-sky NADRE (NADRE_cld) to clear-sky NADRE (NADRE_clr) at the TOA and surface for typical aerosol types and over different geographical regions, where α is surface albedo. TOD and WOD denote the average total and water cloud optical depth, respectively, from MODIS/Terra observations.

of solar flux transmitted through the aerosol layer decreases and so does its radiative effect. In industrial regions examined in this study, the cloud optical depth is largest and values of cloudy-sky NADRE accounts for about 10% and 25% of clear-sky values at the TOA and surface respectively. Over the desert regions, the cloud is thinnest and the ratio of cloudy-sky to clear-sky NADRE is about 0.4 at the TOA and more than 0.5 at the surface. The overlying cloud layer reduces the TOA cooling by a larger percentage than the surface cooling, because the overlying cloud layer can efficiently reflect back the aerosol-upscattered solar radiation and hence increase the solar absorption in the atmosphere.

[24] Because the aerosol optical depth is much smaller than the cloud optical depth, the surface NADRE under a cloudy sky is not sensitive to the position of the cloud layer. On the other hand, the TOA NADRE for a cloudy sky is quite different for the within-cloud versus the below-cloud cases, depending highly on the aerosol single-scattering albedo. The stronger the aerosol absorption, the more efficient the aerosol layer absorbs the reflection from the underlying highly reflective cloud layer. Such absorption can be enhanced by multiple scattering between the cloud and aerosol layer [*Liao and Seinfeld*, 1998]. In comparison to the below-cloud case, this results in a much reduced negative TOA NADRE for weak absorbing aerosols such as dusts and South America biomass burning, and even reverses its sign to a positive TOA NADRE for stronger absorbing aerosols such as South Africa biomass burning aerosols and pollutions. In particular, for the assumed smoke-cloud profile in the within-cloud case, the South Africa biomass burning can cause a TOA heating for cloudy sky, which is over 50% of the clear-sky TOA cooling. Such strong TOA warming is consistent with a case study of South African biomass burning aerosol based on airborne aerosol and cloud measurements [*Keil and Haywood*, 2003].

[25] Simple box models of global aerosol radiative forcing have assumed that [*Charlson et al.*, 1992; *Haywood and Shine*, 1995] the aerosol direct forcing is negligible in a cloudy region and hence the ratio of all-sky to clear-sky NADRE is equal to clear-sky fraction. According to equation (1b), if either the ratio of cloudy-sky to clear-sky NADRE or f_{cld} is close to 0, neglect of the cloudy sky cannot lead to serious error. However, as discussed above, the ratio of cloudy-sky to clear-sky NADRE cannot be neglected in the regions considered in this study and increases with decreasing cloud optical depth. That is, the largest bias will occur for thinner cloud and larger cloud fraction. Any estimate of all-sky aerosol radiative effect is more complicated than that of clear sky because of its dependence on cloud optical depth, cloud fraction, the relative position of cloud and aerosol layer, and aerosol optical properties. For below-cloud cases, all-sky to clear-sky NADRE ratio is generally larger than clear-sky fraction, and therefore the bias by zero-order assumption in simple box models is negative and it increases with decreasing cloud optical depth and clear-sky fraction at the TOA and surface. For the within-cloud case, the bias can be positive at the TOA because of the positive cloudy-sky ADRE, resulting from the strong absorbing aerosols when positioned above the cloud layer, and the positive bias increases with increasing cloud optical depth and aerosol absorption.

4. Summary and Conclusion

[26] The climatology of monthly aerosol direct radiative effect at both the TOA and the surface has been developed

using the AERONET aerosol climatology covering a variety of aerosol regimes, in conjunction with MODIS retrievals of land surface albedo and clouds. The normalized ADRE with respect to optical depth (NADRE) removes much of the dependence of aerosol loading on the aerosol radiative effect; therefore it can flexibly serve as a baseline to evaluate estimates of aerosol direct radiative forcing using satellite observations, model simulations, and their combinations. The data can be provided at request.

[27] The variability of both aerosol types and surface albedos lead to a large range of clear-sky NADRE, varying from about -45 to -15 Wm^{-2} τ^{-1} at the TOA and from -90 to -50 Wm^{-2} τ^{-1} at the surface. Because of its much stronger absorption than that of Amazon smoke, South African smoke on average has a NADRE that is smaller in magnitude by $\sim$35% at the TOA but larger in magnitude by $\sim$38% at the surface. Dust storms in North Africa and Arabian Peninsula influence wide areas where surface albedos range from 0.1 or less to more than 0.3. Such large variations of surface albedo cause large differences in the dust NADRE. The NADRE is -44 and -80 Wm^{-2} τ^{-1} at TOA and surface over oceans, but it decreases respectively to -17 and -48 Wm^{-2} τ^{-1} over highly reflective deserts. The AERONET derived fine-mode aerosols have larger values of single-scattering albedo and smaller values of asymmetry factor than for all-mode aerosols, resulting in a greater (more negative) effect at the TOA but smaller (less negative) effect at the surface. These AERONET derived fine-mode aerosol properties (e.g., absorption or single-scattering albedo) may be different from those of anthropogenic aerosol properties. More efforts are necessary to explore how the fine-mode fraction obtained recently from ground-based and satellite measurements could be used to optimally estimate the anthropogenic aerosol forcing.

[28] The effect of clouds on the ADRE is usually not negligible for the observed cloud optical thickness but is not easily quantified because of its dependence on vertical profiles of aerosol and cloud. The surface NADRE is found to be less sensitive to the position of the cloud layer than that at the TOA. When a portion of aerosol is above the cloud layer, the TOA cooling by weakly absorbing aerosols is much reduced and can even be a positive value (TOA heating) for strongly absorbing aerosols. In particular, if half of the highly absorbing smoke over South Africa were elevated above warm clouds, the TOA would be a heating with a magnitude that was over 50% of the clear-sky TOA cooling.

[29] It is challenging to validate our calculations because of a lack of independent ground-based measurements and inconsistency in spatial coverage. Satellite measurements of fluxes such as those from CERES currently don't derive aerosol radiative forcing over land because of difficulties in quantifying large and heterogeneous surface reflection. We compare AERONET NADRE with some measurement-based estimates of pollutions over east United States, Europe and east Asia, and dust over tropical North Atlantic. AERONET shows good agreement of 5–15% difference with estimations over Mediterranean Area [*Markowicz et al.*, 2002], rural East China at the TOA [*Xu et al.*, 2003] and west coast of North Africa at the surface [*Li et al.*, 2004], while relatively large discrepancies of $\sim$30–60% in the east United States [*Kinne and Pueschel*, 2001], rural east China at the surface [*Xu et al.*, 2003] and west coast of North Africa at the TOA [*Li et al.*, 2004]. A more thorough comparison with model simulations, model-satellite integrations and intensive field measurements will be addressed in a paper by *Yu et al.* [2005].

[30] **Acknowledgments.** We are grateful to Yoram Kaufman, Mian Chin, and Lorraine Remer for their insightful suggestions and David Giles for providing AERONET data. We thank reviewers for their helpful comments and suggestions. Our thanks are extended to AERONET and MODIS scientists in collecting and processing data. The work was supported by NASA NNG04GB89G to Georgia Tech and by funding to Yoram Kaufman and Mian Chin of GSFC for generating the synthesis and assessment products of aerosols for the Climate Change Science Program (CCSP).

References

Ackerman, A. S., O. B. Toon, D. E. Stevens, A. J. Heymsfield, V. Ramanathan, and E. J. Welton (2000), Reduction of tropical cloudiness by soot, *Science*, *288*, 1042–1047.

Albrecht, B. A. (1989), Aerosols, cloud microphysics, and fractional cloudiness, *Science*, *245*, 1227–1230.

Anderson, T. L., R. J. Charlson, S. E. Schwartz, R. Knutti, O. Boucher, H. Rodhe, and J. Heintzenberg (2003a), Climate forcing by aerosols—A hazy picture, *Science*, *300*, 1103–1104.

Anderson, T. L., R. J. Charlson, D. M. Winker, J. A. Ogren, and K. Holmén (2003b), Mesoscale variations of tropospheric aerosols, *J. Atmos. Sci.*, *60*, 119–136.

Anderson, T. L., et al. (2005), An "A-Train" strategy for quantifying direct aerosol forcing of climate, *Bull. Am. Meteorol. Soc.*, in press.

Bohren, C. F., and D. R. Huffman (1983), *Absorption and Scattering of Light by Small Particles*, John Wiley, Hoboken, N. J.

Boucher, O. (1998), On aerosol direct shortwave forcing and Henyey-Greenstein phase function, *J. Atmos. Sci.*, *55*, 128–134.

Boucher, O., and D. Tanre (2000), Estimation of the aerosol perturbation to the Earth's radiative budget over oceans using POLDER satellite aerosol retrievals, *Geophys. Res. Lett.*, *27*, 1103–1106.

Boucher, O., et al. (1998), Intercomparison of models representing direct short-wave radiative forcing by sulfate aerosols, *J. Geophys. Res.*, *103*, 16,979–16,998.

Chameides, W. L., et al. (1999), A case study of the effects of atmospheric aerosols and regional haze on agriculture: An opportunity to enhance crop yields in China through emission controls?, *Proc. Natl. Acad. Sci.*, *96*, 13,626–13,633.

Charlson, R. J., S. E. Schwartz, J. M. Hales, R. D. Cess, J. A. Coakley, J. Hansen, and D. J. Hofmann (1992), Climate forcing by anthropogenic aerosols, *Science*, *255*, 423–430.

Chin, M., et al. (2002), Tropospheric aerosol optical thickness from the GOCART model and comparisons with satellite and Sun photometer measurements, *J. Atmos. Sci.*, *59*, 461–483.

Chou, M.-D., P.-K. Chan, and M. Wang (2002), Aerosol radiative forcing derived from SeaWiFS-retrieved aerosol optical properties, *J. Atmos. Sci.*, *59*, 748–757.

Coakley, J. A., R. D. Cess, and F. B. Yurevich (1983), The effect of tropospheric aerosols on the Earth's radiation budget: a parameterization for climate models, *J. Atmos. Sci.*, *40*, 116–138.

Collins, W. D., et al. (2002), Simulation of aerosol distributions and radiative forcing for INDOEX: Regional climate impacts, *J. Geophys. Res.*, *107*(D19), 8028, doi:10.1029/2000JD000032.

Delmas, R. A., P. Loudjani, A. Podaire, and J.-C. Menaut (1991), Biomass burning in Africa: An assessment of annually burned biomass, in *Global Biomass Burning: Atmospheric, Climatic, and Biospheric Implications*, edited by J. S. Levine, pp. 126–132, MIT Press, Cambridge, Mass.

Dickinson, R. E. (1983), Land surface processes and climate-surface albedos and energy balance, *Adv. Geophys.*, *25*, 305–353.

Dickinson, R. E., A. Henderson-Seller, and P. J. Kennedy (1993), Biosphere-Atmosphere Transfer Scheme (BATS) version 1e as coupled to the NCAR community model, *Tech. Note NCAR/TN-387+STR*, 72 pp., Natl. Cent. of Atmos. Res., Boulder, Colo.

Dubovik, O., and M. D. King (2000), A flexible inversion algorithm for retrieval of aerosol optical properties from Sun and sky radiance measurements, *J. Geophys. Res.*, *105*, 20,673–20,696.

Dubovik, O., et al. (2000), Accuracy assessments of aerosol optical properties retrieved from AERONET Sun and sky-radiance measurement, *J. Geophys. Res.*, *105*, 9791–9806.

Dubovik, O., et al. (2002), Variability of absorption and optical properties of key aerosol types observed in worldwide locations, *J. Atmos. Sci.*, *59*, 590–608.

Eck, T. F., et al. (2003), High aerosol optical depth biomass burning events: A comparison of optical properties for different source regions, *Geophys. Res. Lett.*, *30*(20), 2035, doi:10.1029/2003GL017861.

Fu, Q., and K. N. Liou (1993), Parameterization of the radiative properties of cirrus clouds, *J. Atmos. Sci.*, *50*, 2008–2025.

Hansen, J., M. Sato, and R. Ruedy (1997), Radiative forcing and climate response, *J. Geophys. Res.*, *102*, 6831–6864.

Haywood, J., and O. Boucher (2000), Estimates of the direct and indirect radiative forcing due to tropospheric aerosols: A review, *Rev. Geophys.*, *38*, 513–543.

Haywood, J. M., and K. P. Shine (1995), The effect of anthropogenic sulfate and soot on the clear-sky planetary radiation budget, *Geophys. Res. Lett.*, *22*, 603–606.

Haywood, J. M., and K. P. Shine (1997), Multi-spectral calculations of the radiative forcing of tropospheric sulfate and soot aerosols using a column model, *Q. J. R. Meteorol. Soc.*, *123*, 1907–1930.

Hess, M., et al. (1998), Optical properties of aerosols and clouds: The software package OPAC, *Bull. Am. Meteorol. Soc.*, *79*, 831–844.

Holben, B. N., et al. (1998), AERONET—A federated instrument network and data archive for aerosol characterization, *Remote Sens. Environ.*, *66*, 1–16.

Holben, B. N., et al. (2001), An emerging ground-based aerosol climatology: Aerosol optical depth from AERONET, *J. Geophys. Res.*, *106*, 12,067–12,097.

Intergovernmental Panel on Climate Change (2001), Radiative forcing of climate change, in *Climate Change 2001*, pp. 351–405, Cambridge Univ. Press, New York.

Jin, Z., T. P. Charlock, and K. Rutledge (2002), Analysis of broadband solar radiation and albedo over the ocean surface at COVE, *J. Atmos. Oceanic Technol.*, *19*, 1585–1601.

Jin, Z., et al. (2004), A parameterization of ocean surface albedo, *Geophys. Res. Lett.*, *31*, L22301, doi:10.1029/2004GL021180.

Kaufman, Y. J., D. Tanre, and O. Boucher (2002), A satellite view of aerosols in the climate system, *Nature*, *419*, 215–223.

Keil, A., and J. M. Haywood (2003), Solar radiative forcing by biomass burning aerosol particles during SAFARI 2000: A case study based on measured aerosol and cloud properties, *J. Geophys. Res.*, *108*(D13), 8467, doi:10.1029/2002JD002315.

King, M. D., et al. (2003), Cloud and aerosol properties, precipitable water and profiles of temperature and water vapor from MODIS, *IEEE Trans. Geosci. Remote Sens.*, *41*, 442–458.

Kinne, S., and R. Pueschel (2001), Aerosol radiative forcing for Asian continental outflow, *Atmos. Environ.*, *35*, 5019–5028.

Koren, I. Y., Y. J. Kaufman, L. A. Remer, and J. V. Martins (2004), Measurement of the effect of Amazon smoke on inhibition of cloud formation, *Science*, *303*, 1342–1345.

Li, F., A. M. Vogelmann, and V. Ramanathan (2004), Dust aerosol radiative forcing measured from space over the western Africa, *J. Clim.*, *17*(13), 2558–2571.

Liao, H., and J. H. Seinfeld (1998), Effect of clouds on direct aerosol radiative forcing of climate, *J. Geophys. Res.*, *103*, 3781–3788.

Lucht, W., A. H. Hyman, A. H. Strahler, M. J. Barnsley, P. Hobson, and J.-P. Muller (2000), A comparison of satellite-derived spectral albedos to groundbased broadband albedo measurements modeled to satellite spatial scale for a semi-desert landscape, *Remote Sens. Environ.*, *74*, 85–98.

McClatchey, R. A., et al. (1972), Optical properties of the atmosphere, 3rd ed., *Rep. AFCRL-72-0497*, Air Force Cambridge Res. Lab., Hanscom Air Force Base, Mass.

Platnick, S., et al. (2003), The MODIS cloud products: Algorithms and examples from Terra, *IEEE Trans. Geosci. Remote Sens*, *41*, 459–473.

Ramanathan, V., P. J. Crutzen, J. T. Kiehl, and D. Rosenfeld (2001), Aerosols, climate, and the hydrological cycle, *Science*, *294*, 2119–2124.

Remer, L. A., et al. (2005), The MODIS aerosol algorithm, products and validation, *J. Atmos. Sci.*, *62*(4), 947–973.

Rosenfeld, D., and I. M. Lensky (1998), Satellite-based insights into precipitation formation processes in continental and maritime convective clouds, *Bull. Am. Meteorol. Soc.*, *79*, 2457–2476.

Schaaf, C. B., et al. (2002), First operational BRDF, albedo and nadir reflectance products from MODIS, *Remote Sens. Environ.*, *83*, 135–148.

Sellers, P. J., S. O. Los, C. J. Tucker, C. O. Justice, D. A. Dazlich, C. J. Collatz, and D. A. Randall (1996), A revised land surface parameterization (SiB2) for atmospheric GCMs, part II, The generation of global fields of terrestrial biospheric parameters from satellite data, *J. Clim.*, *9*, 706–737.

Smirnov, A., B. N. Holben, T. F. Eck, O. Dubovik, and I. Slutsker (2000), Cloud screening and quality control algorithms for the AERONET database, *Remote Sens. Environ.*, *73*, 337–349.

Tsvetsinskaya, E. A., et al. (2002), Relating MODIS-derived surface albedo to soils and rock types over Northern Africa and the Arabian peninsula, *Geophys. Res. Lett.*, *29*(9), 1353, doi:10.1029/2001GL014096.

Twomey, S. (1977), The influence of pollution on the shortwave albedo of clouds, *J. Atmos. Sci.*, *34*, 1149–1152.

Vermote, E. F., N. E. El Saleous, and C. O. Justice (2002), Atmospheric correction of MODIS data in the visible to middle infrared: First results, *Remote Sens. Environ.*, *83*, 97–111.

Xu, J., M. H. Bergin, R. Greenwald, and P. B. Russell (2003), Direct aerosol radiative forcing in the Yangtze delta region of China: Observation and model estimation, *J. Geophys. Res.*, *108*(D2), 4060, doi:10.1029/2002JD002550.

Yu, H., S. C. Liu, and R. E. Dickinson (2002), Radiative effects of aerosols on the evolution of the atmospheric boundary layer, *J. Geophys. Res.*, *107*(D12), 4142, doi:10.1029/2001JD000754.

Yu, H., R. E. Dickinson, M. Chin, Y. J. Kaufman, B. N. Holben, I. V. Geogdzhayev, and M. I. Mishchenko (2003), Annual cycle of global distributions of aerosol optical depth from integration of MODIS retrievals and GOCART model simulations, *J. Geophys. Res.*, *108*(D3), 4128, doi:10.1029/2002JD002717.

Yu, H., R. E. Dickinson, M. Chin, Y. J. Kaufman, M. Zhou, L. Zhou, Y. Tian, O. Dubovik, and B. N. Holben (2004), Direct radiative effect of aerosols as determined from a combination of MODIS retrievals and GOCART simulations, *J. Geophys. Res.*, *109*, D03206, doi:10.1029/2003JD003914.

Yu, H., et al. (2005), A review of measurement-based assessment of aerosol direct radiative effect and forcing, *Atmos. Chem. Phys.*, *5*, 7647–7768.

Zhang, J., S. A. Christopher, L. A. Remer, and Y. J. Kaufman (2005), Shortwave aerosol radiative forcing over cloud-free oceans from Terra: 2. Seasonal and global distributions, *J. Geophys. Res.*, *110*, D10S24, doi:10.1029/2004JD005009.

R. E. Dickinson and M. Zhou, School of Earth and Atmospheric Sciences, Georgia Institute of Technology, 311 Ferst Dr., Atlanta, GA 30332-0340, USA. (mzhou@eas.gatech.edu)

O. Dubovik and B. N. Holben, NASA Goddard Space Flight Center, Greenbelt, MD 20771, USA.

H. Yu, Goddard Earth Science and Technology Center, NASA Goddard Space Flight Center and University of Maryland Baltimore County, Greenbelt, MD 20771, USA.